Journal of Power Sources 256 (2014) 170–177

Contents lists available at ScienceDirect

Journal of Power Sources

journal homepage: www.elsevier.com/locate/jpowsour

Rapid charge-transfer in polypyrrole–single wall carbon nanotube complex counter electrodes: Improved photovoltaic performances of dye-sensitized solar cells

Benlin He [a], Qunwei Tang [a,*], Jinghuan Luo [a], Qinghua Li [b], Xiaoxu Chen [a], Hongyuan Cai [a]

[a] Institute of Materials Science and Engineering, Ocean University of China, 238 Songling Road, Qingdao 266100, China
[b] National Defense Key Disciplines Laboratory of Light Alloy Processing Science and Technology, Nanchang Hangkong University, Nanchang 330063, China

HIGHLIGHTS

- PPy–SWCNT complexes are employed as CEs of DSSCs.
- The covalent bonds within PPy–SWCNT complexes accelerate the charge transfer.
- A power conversion efficiency of 8.30% is obtained from the PPy–SWCNT complex-based DSSC.
- Reflux technique is promising in synthesizing efficient CE materials.

GRAPHICAL ABSTRACT

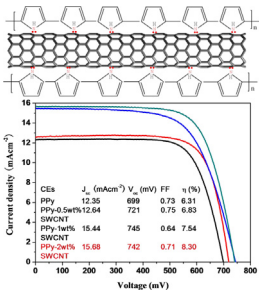

ARTICLE INFO

Article history:
Received 4 November 2013
Received in revised form
17 December 2013
Accepted 14 January 2014
Available online 24 January 2014

Keywords:
Dye-sensitized solar cell
Counter electrode
Polypyrrole–single wall carbon nanotube complex
Reflux technique

ABSTRACT

Dye-sensitized solar cell (DSSC) is a promising solution to global energy and environmental problems because of its clean, high efficiency, good durability, and easy fabrication. However, enhancement of power conversion efficiency and high cost of Pt counter electrode are still significant issues in commercial application of DSSCs. Herein, pyrrole–single wall nanotube (pyrrole–SWCNT) complexes are pioneerly synthesized by a reflux technique and subsequently in-situ polymerized and employed as counter electrodes (CEs) for DSSCs. Different from traditional polypyrrole/SWCNT (PPy/SWCNT) composites, the resultant PPy–SWCNT complexes are expected to fulfill the good electrical-conduction of SWCNT and electrocatalytic behaviors of PPy in accelerating electrochemical activity and charge transfer owing to the covalent bond between PPy (*N* atoms) and SWCNT (*C* atoms). The DSSCs employing PPy–SWCNT complex CEs exhibit significantly enhanced photovoltaic performances, in which a promising power conversion efficiency of 8.30% is obtained from PPy–2 wt‰ SWCNT complex CE in comparison with 6.31% from PPy-only CE. The high conversion efficiency, rapid charge-transfer in combination with simple preparation, relatively low cost, and scalability demonstrates the potential use of PPy–SWCNT complexes in robust DSSCs.

1. Introduction

In the current low-carbon society, dye-sensitized solar cells (DSSCs), electrochemical devices converting solar energy to electricity characterized by a high efficiency, environmental-friendly, inexhaustible, and simple fabrication, have been honored as good candidates for energy crisis [1–3]. A typical DSSC comprises a dye-

* Corresponding author.
E-mail address: tangqunwei@hotmail.com (Q. Tang).

0378-7753/$ – see front matter © 2014 Elsevier B.V. All rights reserved.
http://dx.doi.org/10.1016/j.jpowsour.2014.01.072

sensitized TiO_2 photoanode, a counter electrode (CE), and a redox electrolyte containing I^-/I_3^- redox couples. CE is a crucial component in a DSSC to transfer electrons arriving from external circuit to triiodide in the redox electrolyte. The most commonly used CE in DSSCs is platinum, which is complimented by excellent electrocatalytic activity, high electrical conductivity, and chemical stability [4,5]. However, the high cost of Pt-based materials has been a main obstacle for the commercial application of DSSCs. Therefore, it is a prerequisite to develop low-cost and highly electrocatalytic materials such as conductive polymers, carbon materials, or semiconducting materials as CE alternatives in DSSCs [6–13]. The universalities of these candidates are comparable electrocatalytic performances for triiodide reduction and high electron-transfer ability. Among them, conducting polymers such as polypyrrole (PPy) nanostructures have been considered as one of the most promising CE materials on account of their facile synthesis, high catalytic activity and considerable environmental stability [14–16]. Although PPy nanostructures show considerable merits for application as effective CEs in DSSCs, they suffer from relatively low conductivity in long-range transport, which may cause loss of photocurrent in the cell circuit, and further drag on photovoltaic performances [17].

Carbon nanotubes (CNTs) are honored as excellent electron-transfer materials accompanied with bewitching structure, narrow distribution size, highly accessible surface area, low resistivity, and good stability [18]. The combination of the unique properties of CNTs with hole-conducting PPy makes their combined composite materials interesting in enhancing electrical conduction and therefore conversion efficiency of DSSCs [19,20]. However, low solubility of pristine CNTs in most organic solvents has been the main barrier for their chemical manipulation, quantitative characterization and potential use [18]. To bypass this disadvantage, an efficient key is the functionalization of CNTs with polymers, leading to soluble composite materials [21]. Although surface modification can improve their solubility in some extend, the oxidation process is expected to destroy the well-defined conjugated alignment and therefore weaken the electrical and electrochemical properties. Early works in fabricating PPy/CNT composites are focusing on chemical, physical or electrochemical copolymerization approaches. Niu et al. reported the two-step electropolymerization of PPy/multi-wall carbon nanotube (PPy/MWCNT) composite CE in DSSC [22]. Compared with a reference DSSC using single MWCNT CE of 2.68%, the conversion efficiency was increased by 41.04% using PPy/MWCNT CE. Peng and coworkers prepared PPy/functionalized MWCNT composites and employed as CEs in flexible DSSCs [21], giving a conversion efficiency of 4.04%. Although great efforts have been made on PPy/CNT composite, the current approaches such as chemical polymerization, electropolymerization, drop-casting, or blending are expected to generate two demerits for using CEs of DSSCs: (i) The interfacial resistance between PPy and CNT is relatively high because of their poor contact, which leads to a low charge-transfer kinetics; (ii) Not all the intrinsic performances of CNTs can be maintained after tediously functionality processes. Therefore, PPy/CNT composite CEs do not fulfill the good electrical-conduction of CNT and redox behaviors of PPy in accelerating electrochemical kinetics and charge-transfer, resulting in an unsatisfactory conversion efficiency of DSSCs.

In search for more robust PPy/CNT composite CEs, here we reported that pyrrole could be employed to functionalize and solubilize single wall CNTs (SWCNT) via formation of donor–acceptor complexes by a reflux technique. The resultant pyrrole–SWCNT complexes and therefore PPy–SWCNT complex CEs were thoroughly characterized. Covalent bonding between PPy and SWCNT were expected to accelerate the charge-transfer between them in electrocatalyzing redox couples. Results revealed that the PPy–SWCNT complexes significantly enhanced photovoltaic performances of DSSCs due to their improved charge-transfer kinetics. To the best of our knowledge, no research on reflux synthesis of PPy and SWCNT complexes for use in DSSCs as electrocatalysts has been reported so far. Moreover, the obtained conversion efficiency of 8.30% (AM1.5) is the highest record in DSSCs using conducting polymer/carbon composite CEs.

2. Experimental

2.1. Reflux synthesis of pyrrole–SWCNT complexes

The pyrrole–SWCNT complex was synthesis by a reflux process. In details, three mixtures composing of pyrrole and SWCNTs were sealed in a three-neck flask filled with high-purity N_2 gas. The SWCNT dosages were 0.5, 1, and 2 wt‰. In dark, the mixtures were refluxed for 3 h at 131 °C to obtain the target pyrrole–SWCNT complexes after cooling, which were subsequently stored in a dark and cold atmosphere.

2.2. Deposition of PPy–SWCNT complex CEs

0.25 mL of pyrrole–SWCNT complex was mixed with 37.5 mL of deionized water. Under vigorous agitation, 37.5 mL of $FeCl_3$ aqueous solution (molar ratio of pyrrole to Fe^{3+} was 1: 1) was added to the above mixture. An FTO conductive glass substrate was immersed in the reactant for 2 h at 4 °C. Finally, the FTO substrate was thoroughly rinsed by ethanol and deionized water, and subsequently vacuumly dried at 60 °C for 24 h to obtain anhydrous PPy–SWCNT complex CEs. As a comparison, PPy-only CE was also prepared under the same synthesis conditions.

2.3. Assembly of DSSCs

A layer of TiO_2 colloid with an area of 0.5 × 0.5 cm^2 was coated on FTO conductive glass substrate by a screen printing technique. After air drying, the colloid was calcined at 450 °C for 30 min to obtain TiO_2 nanocrystal anode film with a thickness of around 10 μm. Resultant anodes were further sensitized by immersing into a 0.25 mM ethanol solution of N719 dye ([cis-di(thiocyanato)-*N*,*N*′-bis(2,2′-bipyridyl-4-carboxylic acid)-4-tetrabutylammonium carboxylate]). The DSSCs were fabricated by sandwiching the dye-sensitized TiO_2/SiO_2 anode and FTO supported PPy–SWCNT complex CEs. A redox electrolyte consisted of 100 mM of tetraethylammonium iodide, 100 mM of tetramethylammonium iodide, 100 mM of tetrabutylammonium iodide, 100 mM of NaI, 100 mM of KI, 100 mM of LiI, 50 mM of I_2, and 500 mM of 4-*tert*-butyl-pyridine in 50 mL acetonitrile.

2.4. Electrochemical characterizations

The electrochemical performances were recorded on a conventional CHI660E setup comprising an Ag/AgCl reference electrode, a CE of platinum sheet, and a working electrode of FTO glass supported PPY–SWCNT complex. The cyclic voltammetry (CV) curves were recorded from −0.8 to +1.6 V and back to −0.8 V. Before the measurement, the supporting electrolyte consisting of 50 mM LiI, 10 mM I_2, and 500 mM $LiClO_4$ in acetonitrile was degassed using nitrogen for 10 min. Electrochemical impedance spectroscopy (EIS) measurements were also carried out on the CHI660E Electrochemical Workstation in a frequency range of 0.01 Hz–10^6 kHz and an ac amplitude of 10 mV at room temperature. The resultant impedance spectra were analyzed using the Z-view software. Tafel curves was recorded on the same Workstation by assembling symmetric cell consisting of FTO/PPy–SWCNT

complex|redox electrolyte|FTO/PPy–SWCNT complex and scanning potential window of −1 to 1 V at a scan rate of 10 mV s^{-1}.

2.5. Photovoltaic cells

The photovoltaic test of the DSSCs was carried out by measuring the current–voltage (*J–V*) characteristic curves using an Electrochemical Workstation (CHI660E, Shanghai Chenhua Device Company, China) under irradiation of a simulated solar light from a 100 W Xenon arc lamp (XQ-500 W) in ambient atmosphere. The incident light intensity was controlled at 100 mW cm^{-2} (AM1.5). Each *J–V* curve was scanned for three times and a compromising ones was employed. The fill factor (*FF*) and light-to-electric conversion efficiency (η) were calculated according to the equations:

$$FF = \frac{P_{max}}{J_{SC} \times V_{OC}} = \frac{J_{max} \times V_{max}}{J_{SC} \times V_{OC}} \quad (1)$$

$$\eta(\%) = \frac{P_{max}}{P_{in}} \times 100\% = \frac{J_{SC} \times V_{OC} \times FF}{P_{in}} \times 100\% \quad (2)$$

where J_{SC} was the short-circuit current density (mA cm^{-2}), V_{OC} was the open-circuit voltage (V), P_{in} was the incident light power, P_{max} was the maximum power output, J_{max} (mA cm^{-2}) and V_{max} (V) were the current density and voltage at the point of maximum power output in the *J–V* curves, respectively.

2.6. Other characterizations

The morphologies of the resultant PPy–SWCNT complex were observed with a transmission electron microscopy (TEM; Model JEM-840, JEOL Co., Japan). The UV–vis spectra were measured on a UV-3200 spectrophotometer by dissolving the samples in deionized water. The fluorescence emission spectra were recorded at room temperature using a Fluorolog3-P spectrophotometer. The emission spectrum was collected using a conventional setup at excitation wavelengths of 500 nm. Fourier transform infrared spectrometry (FTIR) spectra were recorded on a PerkinElmer spectrum 1760 FTIR spectrometer. Fourier transformed Raman spectroscopic measurements in the ultraviolet light were performed on a Renishaw inVia Reflex Raman Spectrometer. High-resolution gratings were used to give a spectral resolution of 2 cm^{-1}.

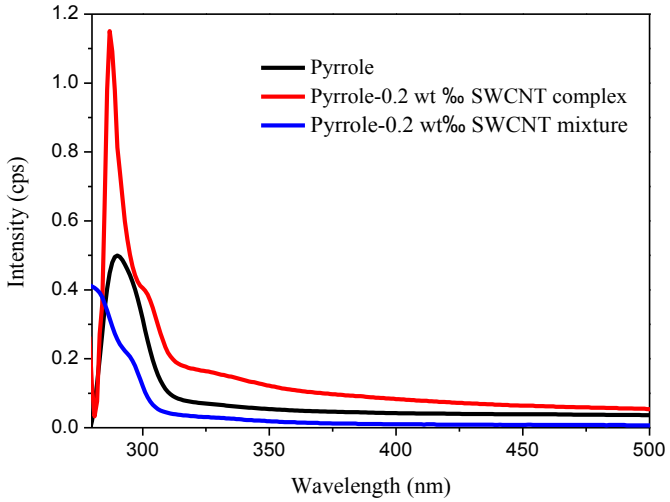

Fig. 2. UV–vis absorption spectra of pure pyrrole, pyrrole–2 wt‰ SWCNT complex, and pyrrole–2 wt‰ SWCNT mixture in acetone.

3. Results and discussion

A prerequisite of fabricating robust PPy–SWCNT complexes with rapid charge-transfer is the successful attachment of pyrrole on SWCNT. Fig. 1a gives fluorescence emission spectra of pure pyrrole and resultant pyrrole–SWCNT complexes diluted with methanol solution and excited at 500 nm. The maximum emissions in methanol were at around 560 and 665 nm, whereas the pure pyrrole fluorescence is generally markedly quenched. Pure SWCNT is believed to give an excitation at 565 nm [23]. The fluorescence excitation spectra of the pyrrole–SWCNT complexes are quite different from the absorption spectra of the individual components, indicating the formation of a new light-absorbing species. It is noteworthy to mention that the red shift of emission maximum, as is shown in Fig. 1b, in an order of acetone, methanol and toluene is the major contributions of their polarities to π–π stacking result from the electrostatic interactions and hydrophobic effects [24].

To reveal the complexing mechanism of pyrrole molecules onto SWCNT, UV–vis adsorption spectra of pure pyrrole, pyrrole–2 wt‰ SWCNT complex, and pyrrole–2 wt‰ SWCNT mixture were diluted in acetone, as is shown in Fig. 2. A single peak is detected at around 280 nm in the spectrum of pyrrole, which is originated from the π–π* transition of the pyrrole rings. In comparison with the UV–vis spectrum of pyrrole–SWCNT mixture, new absorption peaks at 300 and 330 nm are observed, suggesting the successful complexation

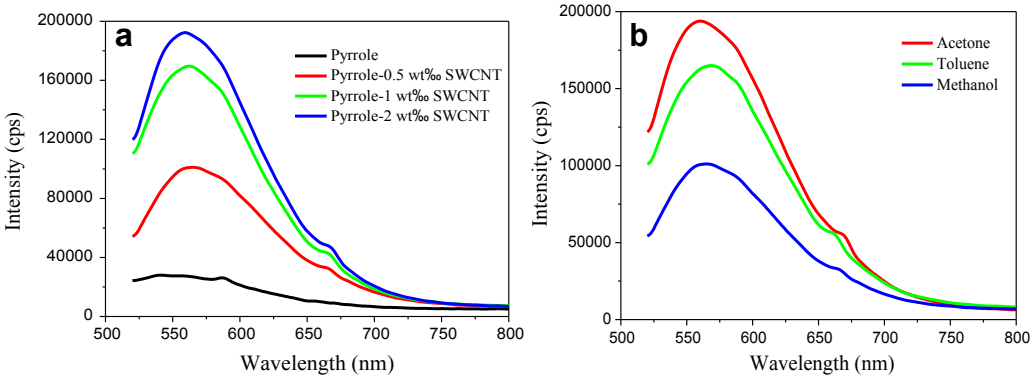

Fig. 1. (a) Emission spectra of pyrrole and pyrrole–SWCNT in methanol at SWCNT dosages of 0.5, 1, and 2 wt‰. (b) Emission spectra of pyrrole–0.5 wt‰ SWCNT complex diluted in organic solvents: acetone, methanol, and toluene. The excitation wavelength was 500 nm.

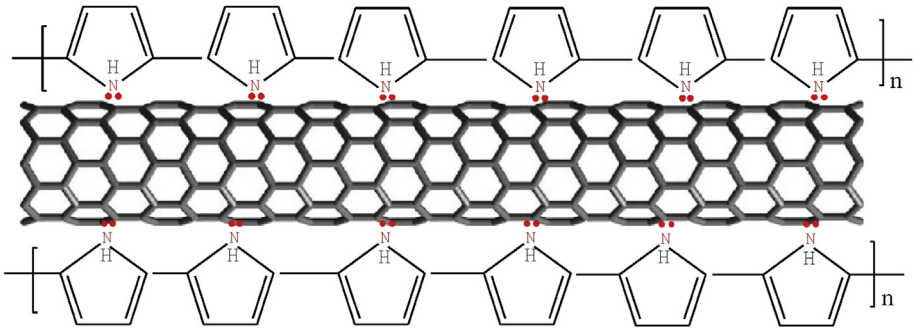

Fig. 3. Proposed complexation mechanism between PPy and SWCNT.

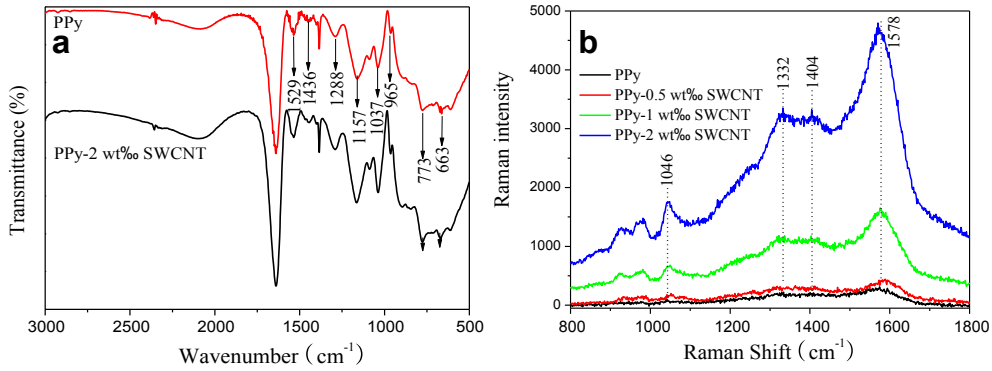

Fig. 4. (a) FTIR and (b) Raman spectra of PPy and PPy–SWCNT complexes.

of pyrrole and SWCNT charge-transfer complex. At elevated temperature, such as 131 °C, SWCNT and pyrrole are believed to form a rapid charge-transfer complex in its ground state because SWCNT is a good electron acceptor, whereas pyrrole is a fairly good electron donor, as evidenced by the appearance of the new absorptions. Originating from pyrrole monomers, they suffer from dimmers, trimers, oligomers and conjugated PPy in the presence of Fe^{3+}. As shown in Fig. 3, each imine group (–NH–) has a lone-electron pair which can share with a carbon atom in conjugation structure of SWCNT (–C=) to form a covalent bond. There is a consensus that the chemical bonding between PPy and SWCNT can significantly accelerate the charge transfer. Furthermore, researches validate that the resultant PPy chains are intertwisted to form agglomerated nanoparticles in traditional chemical polymerization because of the strong intramolecular and intermolecular hydrogen bonding, which resulting in the poor electron delocalization, charge transfer and therefore the electrical and electrochemical performances. The parallel bonding also enhances the well-aligned arrangement of PPy chains along the surface of SWCNTs, which is expected to give extraordinary synergistic effect in accelerating charge transfer.

Fig. 4a provides the reference FTIR spectra of bared PPy and PPy–0.5 wt‰ SWCNT complexes. The peaks at 1529 and 1436 cm^{-1} are from the fundamental stretching vibrations of pyrrole rings. The bands at 1288, 1037 and 773 cm^{-1} can be assigned to the C–N stretching, C–H deformation vibrations and C–H wagging vibrations, respectively. The presence of strong bands at about 1157 and 965 cm^{-1} indicates the formation of doped PPy [25]. The low absorption band at 663 cm^{-1} is due to C–H out of plane bending of pyrrole moiety in PPy [26]. All the characteristic bands of PPy are reserved in the spectrum of PPy–2 wt‰ SWCNT complex. The band shift is a signal of covalent interactions between PPy and SWCNT [27], which is expected to give a facile electron transport between PPy and SWCNT.

Fig. 4b shows Raman spectra of pure PPy and PPy–SWCNT complexes. All spectra of complexes show typical SWCNT features for the tangential (*D* band) and radial (*G* band) breathing modes at

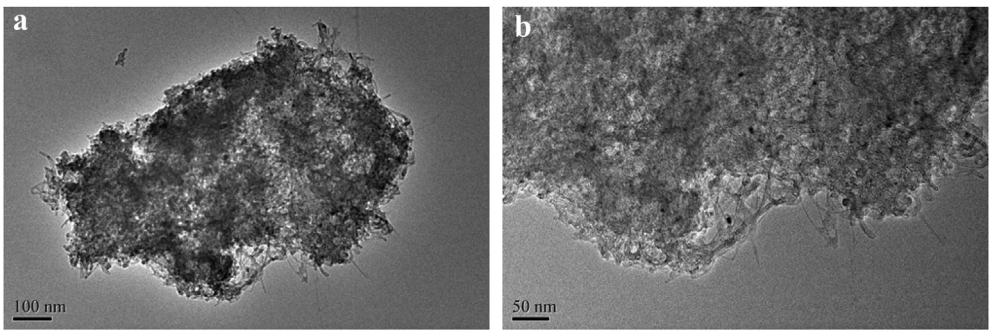

Fig. 5. TEM images of PPy–2 wt‰ SWCNT complex at (a) low- and (b) high-magnifications.

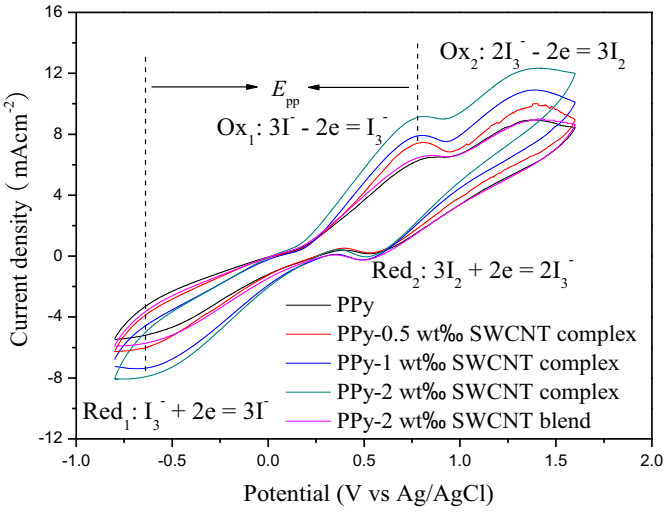

Fig. 6. CV curves of PPy-only and PPy–SWCNT complex CEs toward I^-/I_3^- redox species recorded at a scan rate of 100 mV s^{-1}.

Table 1
Electrochemical parameters from PANi and PANi–SWCNT complex CEs.

CEs	E_{ox1} (V)	E_{red1} (V)	J_{ox1} (mA cm^{-2})	J_{red1} (mA cm^{-2})	E_{pp} (V)	$J_{ox1}/\lvert J_{red1}\rvert$	D_n (cm^{-2} s^{-1})
PPy	0.85	−0.76	6.54	−5.38	1.61	1.22	4.02E-6
PPy–0.5 wt‰ SWCNT	0.82	−0.75	7.54	−6.20	4.57	1.22	7.11E-6
PPy–1 wt‰ SWCNT	0.81	−0.71	8.15	−7.31	1.52	1.12	1.12E-5
PPy–2 wt‰ SWCNT	0.78	−0.70	9.16	−8.14	1.48	1.12	1.19E-5

1332 and 1578 cm^{-1}, respectively [15]. The increase in relative intensity of the *D* band in PPy–SWCNT complexes is a reflection of elevating SWCNT dosage. Two bands at 1046 and 1404 cm^{-1}, reflecting the electrical conductivity of PPy [28], are attributed to C–H in-plane and ring stretching, respectively. The intensities of these two bands increase with the elevation of SWCNT dosage in PPy–SWCNT complexes, indicating the enhancement of electrical behaviors of the PPy–SWCNT complexes.

Fig. 5 shows the typical TEM images of PPy–2 wt‰ SWCNT complex. Plenty of fibrous nanostructures are observed and there is not the detection of PPy aggregations, indicates that pyrrole monomers have been successfully covalently bonded onto SWCNT in a reflux process. Therefore, the molecular conformation of PPy chains is extended along SWCNTs, resulting in good electron dislocation, long-range ordering, and therefore facile electron transfer between PPy and SWCNT.

To explore the electrocatalytic activity of PPy–SWCNT complexes toward I^-/I_3^- redox species, we record the CV curves of the resultant complex CEs in liquid electrolyte with PPy-only CE as a reference, as is shown in Fig. 6. The peak positions and shapes of the CV curves from PPy–SWCNT complex CEs are very similar to those of Pt and PPy-only CE, revealing that PPy–SWCNT complex CEs have a similar electrocatalytic activity to Pt CE. Considering that the task of CE is a mediator of electroreducing redox species in regenerating dye molecules after electron injection in a liquid-state DSSC. The electroreduction reaction of $I_3^- + 2e \rightarrow 3I^-$ can be employed to elevate the electrocatalytic activity of PPy–SWCNT complex CEs [21]. Notably, the combination of SWCNT with PPy significantly increases the peak current density. The higher peak current densities suggest an enhanced electroreductive behavior to I^-/I_3^- redox. It is noteworthy to mention that the SWCNT dosage has a promotion effect on enhancing electrocatalytic activity because of the incremental quantity in bonding sites for rapid charge-transfer. As a reference, the PPy–2 wt‰ SWCNT blend CE is also provided. Apparently, the peak intensity attribution to reduction of triiodides of PPy–2 wt‰ SWCNT blend CE is higher than that of pure PPy but lower than PPy–0.5 wt‰ SWCNT complex, not to mention PPy–2 wt‰ SWCNT complex. The result suggests that the bonding sites between PPy and SWCNT can accelerate the charge-transfer ability and therefore electrocatalytic activity of CEs. Moreover, the ratio of $J_{ox1}/|J_{red1}|$ is a parameter to elevate the reversibility of the redox reaction toward I^-/I_3^-. The obtained value from PPy–2 wt‰ SWCNT complex CE is closer to 1.0 (Table 1). Considering that the E_{pp} (peak-to-peak separation) is higher than 1000 mV, the reversibility of redox reaction by PPy–2 wt‰ SWCNT complex CE is better among three CEs. The rapid recovery of iodides to their ground state facilitates the participation in subsequent circles and improves the long-term stability. To elucidate the relationship between increased bonding sites and diffusion of iodide in a complex CE, Randles–Sevcik theory is employed and presented [29,30]:

$$J_{red} = Kn^{1.5}ACD_n^{0.5}v^{0.5} \quad (3)$$

where J_{red} is the peak current density of Red_1 (mA cm^{-2}), *K* is 2.69×10^5, *n* is the number of electrons of reduction reaction, *A* is the electrode area (cm^2), *C* represents the bulk concentration of I_3^- (mol L^{-1}), and D_n is the diffusion coefficient (cm^{-2} s^{-1}). The diffusivity of PPy-only CE is 4.02×10^{-6} cm^{-2} s^{-1} which is comparable to 4.92×10^{-6} cm^{-2} s^{-1} of poly(3,4-ethylenedioxythiophene) (PEDOT) and 2.55×10^{-6} cm^{-2} s^{-1} of Pt

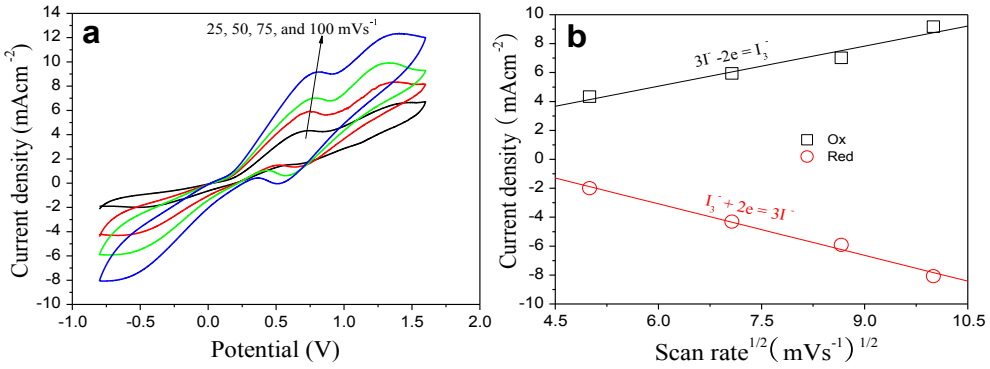

Fig. 7. (a) CV curves of PPy–2 wt‰ SWCNT complex CE for I^-/I_3^- redox species at different scan rates (from inner to outer: 25, 50, 75, and 100 mV s^{-1}), and (b) relationship between peak current density and square root of scan rates.

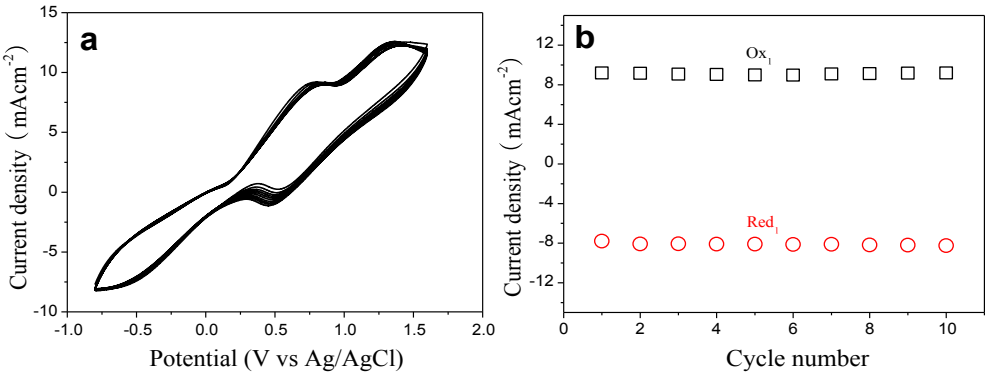

Fig. 8. (a) A total of 10 consecutive CVs toward I^-/I_3^- species using the PPy–2 wt‰ SWCNT CE at a scan rate of 100 mV s^{-1}, (b) plots of redox peak current density as a function of cycle number from PPy–2 wt‰ SWCNT CE.

CEs [29]. There is an ascending trend in increasing SWCNT dosage (7.11×10^{-6} cm^{-2} s^{-1} of PPy–0.5 wt‰ SWCNT complex, 1.12×10^{-5} cm^{-2} s^{-1} of PPy–1 wt‰ SWCNT complex) and it is 1.19×10^{-5} cm^{-2} s^{-1} for PPy–2 wt‰ SWCNT complex CE which is much higher than 9.95×10^{-6} cm^{-2} s^{-1} for PPy-only CE [30]. Results indicate that the elevated bonding sites between PPy and SWCNT can accelerate both charge transfer and iodide species within PPy–SWCNT complex CEs.

From the stacking CV curves of PPy–2 wt‰ SWCNT complex CE at different scan rates, one can find an outward extension of all the peaks (Fig. 7a). By plotting peak current density corresponding to $I_3^- \leftrightarrow I^-$ versus square root of scan rate, as shown in Fig. 7b, linear relationships are observed. This result indicates the redox reaction on the surface of the PPy–2 wt‰ SWCNT complex CE is controlled by ionic diffusion in the electrolyte, and the transfer rate of both electrons and ions are fast enough for the reduction rate of I_3^- on the surface of PPy–2 wt‰ SWCNT complex CE. This result also suggests that the adsorption of iodide species is hardly affected by the redox reaction on the PPy–2 wt‰ SWCNT complex CE surface and no specific interaction occurred between I^-/I_3^- and the complex CE [21,31].

To evaluate the stability of PPy–2 wt‰ SWCNT CE, ten successive CV cycles from PPy–2 wt‰ SWCNT CE were carried out toward redox reaction of iodides, as shown in Fig. 8a. In the consecutive ten CV cycles, the redox current densities remain unchanged. The correlations between the peak current densities and the cycle numbers are summarized in Fig. 8b. Both redox peak current densities remain stable with increasing the cycle number. This indicates that the PPy–2 wt‰ SWCNT complex has good chemical stability and is tightly bound to the FTO glass surface [29,32].

With an aim of further elucidating the catalytic activities of PPy–SWCNT complex CEs on the reduction of triiodide, EIS experiments were carried out in a symmetric cells fabricated by two identical CEs. Nyquist plots in Fig. 9 illustrate impedance characteristics of PPy-only and PPy–SWCNT complex CEs, in which one semicircle and a tail are observed in each EIS curve. The detected EIS plots are in an agreement with other reports [33,34]. According to the Randles-type circuit (inset of Fig. 9), the intercept on the real axis represents the series resistance (R_s). The arc arises from the charge-transfer resistance (R_{ct}) at CE/electrolyte interface, which changes inversely with the electrocatalytic activity of CEs on the reduction of triiodide, whereas W represents the Nernst diffusion impedance corresponding to the diffusion resistance of I^-/I_3^- redox species. CPE is a constant phase element and is frequently used as a substitute for a capacitor in an equivalent circuit to fit the impedance behavior of the electrical double layer. These electrochemical parameters were obtained by fitting EIS spectra using a Z-view software, as is shown in Table 2, and there is a good agreement between recorded and fitted curves. Both R_s and R_{ct} decrease with increase of SWCNT dosage, indicating an inverse order of electrocatalytic activity. W is of highly dependence on the electrical conduction of PPy–SWCNT complex CE [35]. With increasing of SWCNT dosage, the electrical resistance of CE decreases, which can be confirmed by Fig. 9. Therefore, the W value, diffusion resistance of I^-/I_3^-, is declining on SWCNT content. The conclusions for the electrocatalytic activity and diffusion derived from EIS and CV data are consistent.

To further verify the electrocatalytic activities of the CEs, Tafel polarization curves were performed with the dummy cells similar to those in EIS measurements. Fig. 10 shows the Tafel curves with logarithmic current density (log J) as a function of the voltage. Theoretically, the Tafel curve can be divided into three zones. The curve at very high potential is attributed to the limiting diffusion zone, which depends on the transport of triiodide and iodide in the

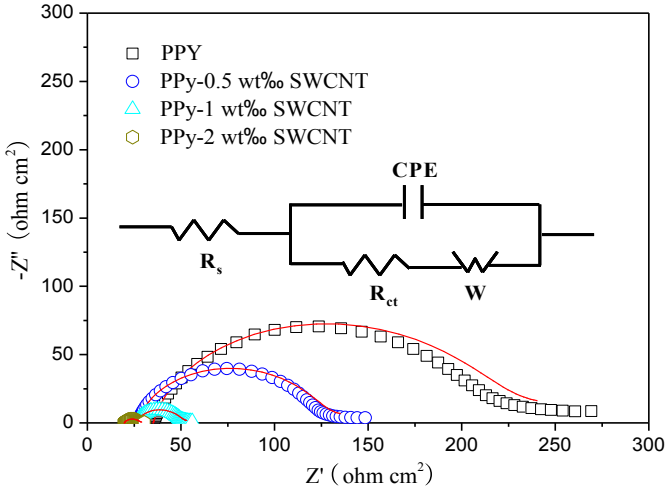

Fig. 9. Nyquist plots for symmetric cells fabricated with PPy-only or PPy–SWCNT complex CEs. The lines express fit results for corresponding EIS data, and the inset gives the equivalent circuit.

Table 2
Parameters for equivalent circuit obtained by fitting EIS data using a Z-view software.

CEs	R_s (Ω cm^2)	R_{ct} (Ω cm^2)	W (Ω cm^2)
PPy	35.22	179.4	29.52
PPy–0.5 wt‰ SWCNT	27.02	40.07	17.91
PPy–1 wt‰ SWCNT	26.61	23.57	5.52
PPy–2 wt‰ SWCNT	19.75	8.15	1.14

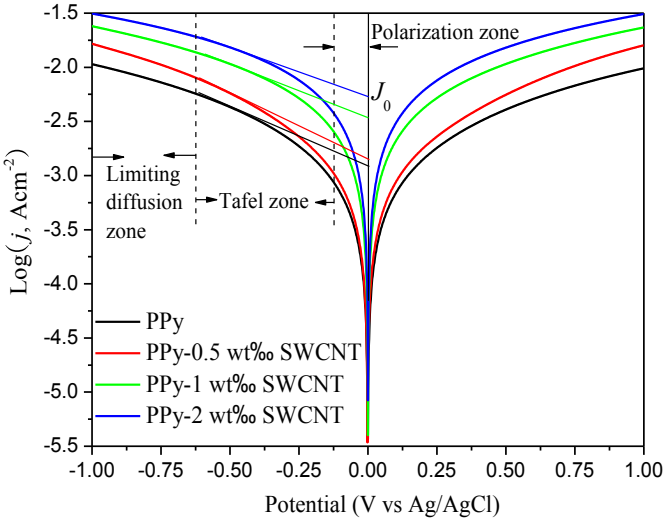

Fig. 10. Tafel polarization curves of symmetrical cells fabricated with PPy-only or PPy–SWCNT complex CEs that are the same as the ones used in EIS experiments.

electrolyte. The curve at relatively low potential but higher than 120 mV corresponds to the Tafel zone, where the voltage is a linear function of log *J*. The curve at very low potential is polarization zone, arising from the electrochemical reaction. In Tafel zone, we can collect information on the exchange current density (J_0, obtained by the intersection of cathodic branch and equilibrium potential line) [36–38]. Since J_0 mainly depends on two factors, the concentration of the oxidized species and the electrocatalytic performance of CE. Evidently, the large slope of cathodic and anodic branches is associated with high J_0, which follows an order of PPy–2 wt‰ SWCNT > PPy–1 wt‰ SWCNT > PPy–0.5 wt‰ SWCNT > PPy, which in an agreement with electrocatalysis toward I^-/I_3^- redox couples. Moreover, as a kinetic component arises due to the charge transfer of CE, J_0 is associated with the R_{ct} by the equation:

$$J_0 = RT/nFR_{ct} \quad (4)$$

where *R* is the universal gal constant, *T* is the absolute temperature, *n* is the number of electrons contributing to the charge transfer at the interface, and *F* is Faraday's constant. Therefore, the EIS and

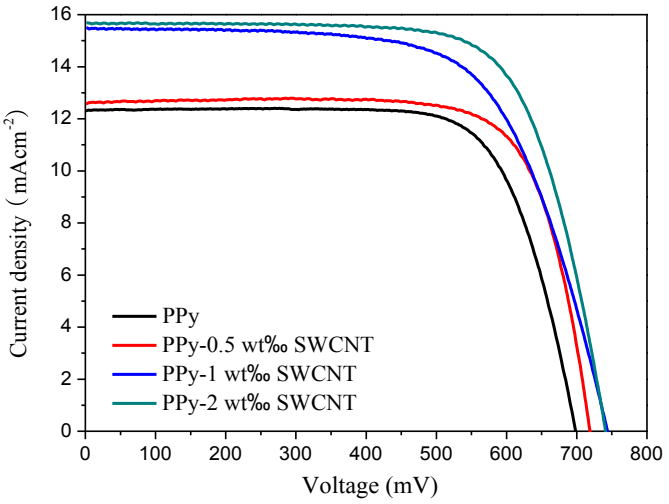

Fig. 11. *J–V* characteristics of DSSCs from pure PPy and PPy–SWCNT complex CEs.

Table 3
Comparison of short-circuit current density (J_{sc}), open-circuit voltage (V_{oc}), fill factor (*FF*), and power conversion efficiency (η) in the resultant DSSCs.

CEs	Photovoltaic parameters			
	J_{sc} (mA cm^{-2})	V_{oc} (mV)	*FF*	η (%)
PPy	12.35	699	0.73	6.31
PPy–0.5 wt‰ SWCNT complex	12.64	721	0.75	6.83
PPy–1 wt‰ SWCNT complex	15.44	745	0.64	7.54
PPy–2 wt‰ SWCNT complex	15.68	742	0.71	8.30

Tafel results match well. In comparison with PPy-only CE, the enhanced J_0 from PPy–SWCNT complex ones derives from the porous structure and rapid charge-transfer, as shown in TEM image and proposed mechanism [39].

Fig. 11 shows the photovoltaic characteristics of DSSCs from pure PPy and PPy–SWCNT complex CEs and the parameters reflecting DSSC properties are summarized in Table 3. The DSSCs employing PPy–SWCNT complex CEs achieve higher J_{sc} than that fabricated using a PPy-only CE. This might be attributed to the good dispersion of PPy–SWCNT complexes, which provides larger active surface areas for I_3^- reduction. The PPy–SWCNT complex, prepared at the optimal condition in this study, significantly improves the charge-transfer ability within CEs, which is evident in the higher J_{sc} observed for the DSSCs. There is a significant enhancement in η of resultant DSSC, and the highest η is 8.30% at 2 wt‰ SWCNT in comparison with that of 6.31% from PPy-only CE. After performing a comprehensive analysis of the DSSCs, it can be concluded that the photovoltaic performance is in agreement with the EIS and Tafel polarization results.

4. Conclusions

In summary, we have demonstrated that the fabrication of PPy–SWCNT complex CEs by a reflux technique is an effective strategy for accelerating the charge transfer within the complexes. New light-absorbing species and absorption bands can be detected from the fluorescence excitation and UV–vis absorption spectra of pyrrole–SWCNT complexes. Covalent bonds between PPy (–NH–) and SWCNT (–C=) are expected to significantly accelerate the charge transfer. EIS, CV, and Tafel measurements have been carried out to determine the enhancement in charge-transfer kinetics and electrocatalytic activity toward iodides. The DSSC from PPy–2 wt‰ SWCNT complex CE provides an impressive power conversion efficiency of 8.30% in comparison with that of 6.31% from PPy-only CE. The research presented here is far from being optimized but these profound advantages along with low-cost synthesis and scalable materials promise the new PPy–SWCNT complex CEs to be strong candidates in robust DSSCs.

Acknowledgments

The authors would like to acknowledge financial supports from Seed Fund from Ocean University of China, Fundamental Research Funds for the Central Universities (201313001, 201312005), Shandong Province Outstanding Youth Scientist Foundation Plan (BS2013CL015), Doctoral Fund of Ministry of Education of China (20130132120023), Shandong Provincial Natural Science Foundation (ZR2011BQ017), and Research Project for the Application Foundation in Qingdao (13-1-4-198-jch).

References

[1] B. O'Regan, M. Grätzel, Nature 353 (1991) 737–740.
[2] Z.Y. Tang, J.H. Wu, Q. Liu, M. Zheng, Q.W. Tang, Z. Lan, J.M. Lin, J. Power Sources 203 (2012) 282–287.

[3] W. Sun, X. Sun, T. Peng, Y. Liu, H. Zhu, S. Guo, X.Z. Zhao, J. Power Sources 201 (2012) 402–407.
[4] M. Grätzel, Nature 414 (2001) 338–344.
[5] A. Hagfeldt, G. Boschloo, L. Sun, L. Kloo, H. Pettersson, Chem. Rev. 110 (2010) 6595–6663.
[6] G.Q. Wang, W. Xing, S.P. Zhuo, J. Power Sources 194 (2009) 568–573.
[7] M.X. Wu, Q.Y. Zhang, J.Q. Xiao, C.Y. Ma, X. Lin, C.Y. Miao, Y.J. He, Y.R. Gao, A. Hagfeldt, T.L. Ma, J. Mater. Chem. 21 (2011) 10761–10766.
[8] H.C. Sun, D. Qin, S.Q. Huang, X.Z. Guo, D.M. Li, Y.H. Luo, Q.B. Meng, Energy Environ. Sci. 4 (2011) 2630–2637.
[9] G.R. Li, F. Wang, Q.W. Jiang, X.P. Gao, P.W. Shen, Angew. Chem. Int. Ed. 49 (2010) 3653–3656.
[10] Q.H. Li, J.H. Wu, Q.W. Tang, Z. Lan, P.J. Li, J.M. Lin, L. Q Fan, Electrochem. Commun. 10 (2008) 1299–1302.
[11] R. Gokhale, S. Agarkar, J. Debgupta, D. Shinde, B. Lefez, A. Banerjee, J. Jog, M. More, B. Hannoyer, S. Ogale, Nanoscale 4 (2012) 6730–6734.
[12] X. Li, L.F. Liu, G.H. Liu, Y.G. Rong, Y. Yang, H. Wang, Z.L. Ku, M. Xu, C. Zhong, H.W. Han, Adv. Funct. Mater. 23 (2013) 3344–3352.
[13] Q. Tang, H. Cai, S. Yuan, X. Wang, J. Mater. Chem. A 1 (2013) 317–323.
[14] S.S. Jeon, C. Kim, J. Ko, S.S. Im, J. Mater. Chem. 21 (2011) 8146–8151.
[15] S. Hou, Z. Lv, H. Wu, X. Cai, Z. Chu, Y. Ma, D. Zou, J. Mater. Chem. 22 (2012) 6549–6552.
[16] C. Bu, Q. Tai, Y. Liu, S. Guo, X. Zhao, J. Power Sources 221 (2013) 78–83.
[17] F. Gong, X. Xu, G. Zhou, Z.S. Wang, Phys. Chem. Chem. Phys. 15 (2013) 546–552.
[18] Y.K. Zhou, B.L. He, W.J. Zhou, H.L. Li, J. Electrochem. Soc. 151 (2004) A1052–A1057.
[19] Y.M. Xiao, J.Y. Lin, J.H. Wu, S.Y. Tai, G.T. Yue, T.W. Lin, J. Power Sources 233 (2013) 320–325.
[20] Z. Yang, T. Chen, R. He, H. Li, H. Lin, L. Li, G. Zou, Q. Jia, H. Peng, Polym. Chem. 4 (2013) 1680–1684.
[21] S. Peng, Y. Wu, P. Zhu, V. Thavasi, S.G. Mhaisalkar, S. Ramakrishna, J. Photochem. Photobiol. A 223 (2011) 97–102.
[22] J. Luo, H.H. Niu, H.L. Wen, W.J. Wu, P. Zhao, C. Wang, X.D. Bai, W. Wang, Mater. Res. Bull. 48 (2013) 988–994.
[23] Z. Qian, C. Wang, H. Feng, C. Chen, J. Zhou, J. Chen, Chem. Commun. 47 (2011) 7167–7169.
[24] C.A. Hunter, Chem. Soc. Rev. 23 (1994) 101–109.
[25] J. Zhang, X.S. Zhao, J. Phys. Chem. C 116 (2012) 5420–5426.
[26] J. Wu, Q. Li, L. Fan, Z. Lan, P. Li, J. Lin, S. Hao, J. Power Sources 181 (2008) 172–176.
[27] H.F. Guo, H. Zhu, H.Y. Lin, J.Q. Zhang, Colloid Polym. Sci. 286 (2008) 587–591.
[28] G. Han, J. Yuan, G. Shi, F. Wei, Thin Solid Films 474 (2005) 64–69.
[29] Y. Xiao, J.Y. Lin, S.Y. Tai, S.W. Chou, G. Yue, J. Wu, J. Mater. Chem. 22 (2012) 19919–19925.
[30] Y. Xiao, J.Y. Lin, W.Y. Wang, S.Y. Tai, G. Yue, J. Wu, Electrochim. Acta 90 (2013) 468–474.
[31] Y. Saito, W. Kubo, T. Kitamura, Y. Wada, S. Yanagida, J. Photochem. Photobiol. A 164 (2004) 153–157.
[32] H. Guo, Y. Li, L. Fan, X. Wu, M. Guo, Electrochim. Acta 51 (2006) 6230–6237.
[33] G.T. Yue, J.H. Wu, Y.M. Xiao, J.M. Lin, M.L. Huang, Electrochim. Acta 67 (2012) 113–118.
[34] L. Chen, W. Tan, J. Zhang, X. Zhou, X. Zhang, Y. Lin, Electrochim. Acta 55 (2010) 3721–3726.
[35] J. Chen, B. Li, J. Zheng, J. Zhao, H. Jing, Z. Zhu, Electrochim. Acta 56 (2011) 4624–4630.
[36] Y. Wang, C. Zhao, M. Wu, W. Liu, T. Ma, Electrochim. Acta 105 (2013) 671–676.
[37] S. Yun, L. Wang, W. Guo, T. Ma, Electrochem. Commun. 24 (2012) 69–73.
[38] M. Wu, X. Lin, Y. Wang, L. Wang, W. Guo, D. Qi, et al., J. Am. Chem. Soc. 134 (2012) 3419–3428.
[39] W. Zeng, G.J. Fang, X.Q. Wang, Q. Zheng, B.R. Li, H.H. Huang, H. Tao, N.S. Liu, W.J. Xie, X.Z. Zhao, D.C. Zou, J. Power Sources 229 (2013) 102–111.